Physical Communication 2 (2009) 296–305

Contents lists available at ScienceDirect

Physical Communication

journal homepage: www.elsevier.com/locate/phycom

Full length article

A novel approach to UWB data detection with symbol-level synchronization☆

Vincenzo Lottici [a,*,1], Zhi Tian [b,2], Geert Leus [c,3]

[a] Department of Information Engineering, University of Pisa, Pisa, Italy

[b] Department of Electrical & Computer Engineering, Michigan Technological University, Houghton, MI, United States

[c] Faculty of Electrical Engineering, Mathematics, and Computer Science, Delft University of Technology, Delft, The Netherlands

ARTICLE INFO

Keywords:
Ultra-wideband communications
Multi-symbol differential detection
Symbol-level synchronization
Sphere decoding

ABSTRACT

Differentially modulated ultra-wideband (UWB) systems have recently attracted a lot of attention since they can avoid the costly channel estimation required by coherent schemes. The conventional differential-detector (DD), however, shows an inevitable 3 dB performance loss and suffers from multiple access and intersymbol interference. Multiple symbol differential detection (MSDD) provides an attractive solution that alleviates the SNR loss, but still calls for accurate timing recovery. In this paper, we show how to relax the severe timing requirements of the MSDD thereby only relying on symbol-level synchronization. Further, the detection complexity can be kept at an affordable level by pursuing a sphere decoding approach. Simulation results corroborate the effectiveness of the proposed system when operating in typical dense multipath propagation scenarios.

1. Introduction

Ultra-wideband (UWB) impulse radios have been attracting a growing interest in the field of next-generation wireless communications [1,2]. Conveying information over a stream of ultrashort pulses at very low spectral density, several attractive features are promised including fine timing resolution, robustness against multipath, high user capacity, coexistence with legacy services via frequency-overlay, low probability of interception and detection and precise positioning capability [1]. These appealing features have designated UWB signaling as a viable candidate to efficiently meet the strict requirements imposed by several applications, such as short-range high-rate indoor connectivity, location-aware wireless networks and low-rate communications with high-resolution ranging [2].

The harsh multipath propagation conditions typically occurring in wireless environments, however, hamper the extensive deployment of UWB systems. Each transmitted pulse, indeed, arrives at the receiver over tens or even hundreds of delayed paths [3], with possibly severe per-pulse shape distortion due to diffraction and scattering effects [4]. In such operating environments, exploiting the rich diversity of UWB channels is evidently revealed as being very difficult, especially in view of the limited affordable receiver complexity. The well-known Rake receiver can collect a significant fraction of the received energy scattered over a dense multipath [5]. But as a matter of fact, its choice is practically impeded by the large required number of correlator-based fingers combined with the intensive computational load involved in the estimation of channel parameters [6]. Viable yet sub-optimal alternatives for efficient energy capture have been recently proposed in the form of transmitted reference (TR), differential

☆ Parts of this paper were presented at the SCVT'2007 Conf. in Nov. 2007 and the ICUWB'2008 Conf. in Sept. 2008.

* Corresponding author. Tel.: +39 050 2217 536; fax: +39 050 2217 522.
E-mail addresses: vincenzo.lottici@iet.unipi.it (V. Lottici), ztian@mtu.edu (Z. Tian), g.j.t.leus@tudelft.nl (G. Leus).

1 Supported by the FP7 Network of Excellence in Wireless COMmunications NEWCOM++ (contract n. 216715).

2 Supported by US NSF CAREER grant CCF-0238174.

3 Supported in part by NWO-STW under the VIDI program (DTC.6577).

1874-4907/$ – see front matter © 2009 Elsevier B.V. All rights reserved.
doi:10.1016/j.phycom.2009.08.009

detector (DD) schemes and their variants [7–10]. In the former, the received waveform resulting from "information-free" reference pulse(s) is used as noisy template in a simple correlation receiver for data detection, whereas in the latter differential encoding of information data allows one to detect the current symbol using as noisy template a replica of the signal waveform received within the previous symbol interval. These detectors can gather energy from all multipath components bypassing costly path-by-path channel estimation, but still suffer from several considerable drawbacks, among which the fact that the template waveform recovered from the received signal is neither noise-free nor interference-free. As a result, both of them experience poor detection performance when operating in the presence of severe multiple access and inter-symbol interference.

The need for circumventing the inherent weaknesses of the TR and DD methods has thus prompted the development of improved non-coherent receivers. A recent solution is based on the idea of jointly detecting a block of consecutive differentially-encoded symbols experiencing the same unknown channel, which is termed as multiple symbol differential detection (MSDD) [11–13]. The efficacy of the MSDD approach is confirmed by the considerable resilience to severe multipath fading and multiple access interference (MAI). The detection performance obtainable by the MSDD at a reasonable complexity exhibits only a small gap from the (impractical) conventional Rake processing, say around 3–4 dB, and favorably combines with the capability of working independently of the pulse shape distortion and the knowledge of the channel response. The advantages of the MSDD can be attained, however, only provided that timing information is appropriately recovered from the received signal [13]. But designing synchronization algorithms for UWB receivers (that in practice means to identify at frame level where the first frame in each symbol starts, and then, to find at the pulse level where a pulse is located within a frame) is quite a real and demanding task, exacerbated also by the adoption of extremely narrow and low-amplitude pulses. This is demonstrated by the large effort spent so far in the literature on this topic, for example, [14–19]. These synchronization techniques offer adequate estimation accuracy in the presence of both dense multipath and severe MAI level. Nevertheless, the strong limitation they incur is the necessity of training sequences or accumulation of long segments of the received signal that often combines with a heavy computational load. Clearly, such issues disagree with the UWB philosophy that calls for as simple and fast as possible receiver processing schemes.

Starting from the baseline illustrated above, one is well motivated to make a further step toward an efficient detector that ensures competitive performance levels at even lower complexity while avoiding both channel estimation and accurate timing synchronization. To this end, this paper develops a new UWB detector within the MSDD framework under the relaxed assumption that timing information is roughly acquired at the symbol level only, or in other words, the initial timing resolution can be as large as one symbol period [20]. Bypassing accurate timing estimation, we come up with a novel multi-symbol detection scheme, in the sequel referred to as MSDD based on symbol-level synchronization or SLS-MSDD for short, that departs from previous works thanks to the following distinct features.

(1) The SLS-MSDD adopts an optimization criterion based on the generalized likelihood ratio test (GLRT), in which the likelihood function is maximized not only with respect to the symbols to be searched for, but also over all the finite-energy received template waveforms. As such, both the channel response and the timing offset are treated by the receiver as unknown quantities and hence do not need to be explicitly acquired.
(2) By virtue of the GLRT-based optimization approach, the expensive channel estimation task is bypassed without affecting the received energy capture mechanism.
(3) Dealing implicitly with the mistiming effect (within the detection process itself) allows detection of the burst data only from the *easy-to-get* information of where the symbol boundaries are roughly located, rather than requiring *costly* timing synchronization at frame or even at pulse level.[4]
(4) The implementation of the SLS-MSDD scheme via exhaustive search exhibits exponential complexity that quickly becomes impractical as the burst length increases. Consequently, in order to exploit the performance advantages expected at large data block sizes,[5] a proper reformulation of the proposed detector based on sphere decoding (SD) [23] suggests a fast iterative scheme that attains the desired performance of the original formulation but at an appealing polynomial complexity.

The fast SLS-MSDD algorithm can conveniently make salient tradeoffs in performance versus complexity via the choice of the data block size and the (floating-point or integer-based) arithmetic format adopted in the computation of the SD metrics. Extensive simulation results under typical multipath indoor propagation environments corroborate the effectiveness of our scheme.

The rest of the paper is organized as follows. Section 2 presents the UWB system model, Section 3 derives the novel SLS-MSDD receiver, while the fast algorithm based on SD is developed in Section 4. Section 5 is devoted to evaluating performance and complexity via computer simulations, followed by concluding remarks in Section 6.

2. System model

In UWB impulse radio signaling, each symbol is conveyed over a block of N_f frames with one pulse $p(t)$ per frame. The symbol, frame and pulse durations are denoted as T_s, T_f and T_p respectively, satisfying $T_s = N_f T_f$, $T_f \gg T_p$, and T_p being on the order of (sub-)nanoseconds.

[4] Accurate timing recovery is mandatory in conventional UWB receivers so as to maintain adequate system throughput and capacity performance [21,22].

[5] This is due to improved averaging over the noise and MAI components.

Concurrent channel access is enabled by employing user-specific pseudo-random time hopping (TH) codes $\{c_j\}_{j=0}^{N_f-1} \in [0, N_c - 1]$, which time-shifts pulse positions at multiples of the chip period T_c, with $N_c T_c < T_f$. Assume that pulse amplitude modulation (PAM) is adopted and the independent information-bearing symbols $a_i \in \{\pm 1\}$ are transformed into the channel symbols $b_i \in \{\pm 1\}$ through the differential encoding rule $b_i = a_i b_{i-1}$. The transmitted signal relevant to a burst of M information symbols can be written as

$$x(t) = \sum_{i=0}^{M} b_i p_s(t - iT_s), \tag{1}$$

where the symbol-long waveform $p_s(t)$ is

$$p_s(t) = \sum_{j=0}^{N_f-1} p(t - jT_f - c_j T_c). \tag{2}$$

After traveling through a slow-fading multipath channel, assumed to be time-invariant within each block and with L paths each with gain α_l and delay τ_l, the received signal in the interval $0 \le t \le (M+1)T_s$ can be written according to (1) as

$$y(t) = \sum_{i=0}^{M} b_i u_s(t - iT_s - \tau) + w(t). \tag{3}$$

The timing offset τ in (3) is the delay of the first path due to the signal propagation from the transmitter to the receiver, the additive noise component $w(t)$ accounts for the contribution of both the thermal noise and MAI, whereas

$$u_s(t) = \sum_{j=0}^{N_f-1} u(t - jT_f - c_j T_c) \tag{4}$$

is the received symbol-level waveform with non-zero support less than T_s, i.e., ISI-free condition is satisfied, depending on the channel impulse response through

$$u(t) = \sum_{l=0}^{L-1} \alpha_l p(t - \tau_{l,0}), \tag{5}$$

where $\tau_{l,0} \triangleq \tau_l - \tau$.

3. Multiple symbol differential detection with symbol-level synchronization

In this section, we derive the structure of a novel MSDD scheme that aims at recovering M consecutive differentially-encoded information symbols $\mathbf{a} \triangleq [a_1, a_2, \ldots, a_M]^{\mathrm{T}}$ from the received signal $y(t)$ in the interval $0 \le t \le (M+1)T_s$. The following main assumptions will be adopted: (i) the timing offset τ is assumed to be within the interval $[0, T_s)$, thus meaning that the timing information is acquired at symbol-level *only* through some form of (rough) coarse synchronization; (ii) the data block size $(M+1)T_s$ is smaller than the channel coherence time so that hereinto the channel is considered as time-invariant; (iii) the channel impulse response is unknown and will not be explicitly estimated during detection in order to reduce the overall receiver complexity; (iv) the composite noise $w(t)$, including both ambient noise and MAI, is modeled as a wide sense stationary white Gaussian process with two-sided power spectral density $\mathcal{N}_0/2$.

To cope with the lack of accurate pulse-level timing information, our basic idea is to partition the received symbol-level waveform $u_s(t)$ in (4) into the two segments

$$u_s^{(0)}(t) \triangleq \begin{cases} 0, & t \in [0, \tau) \\ u_s(t - \tau), & t \in [\tau, T_s) \end{cases},$$

$$u_s^{(1)}(t) \triangleq \begin{cases} u_s(t + T_s - \tau), & t \in [0, \tau) \\ 0, & t \in [\tau, T_s) \end{cases}, \tag{6}$$

both of which rely on the unknown timing offset τ. Making use of (6) and expressing the differentially-encoded channel symbol as $b_i = b_0 \prod_{k=1}^{i} a_k$, $i > 0$, the received signal (3) can be put in the following alternative form

$$\begin{aligned} y(t) &= \sum_{i=0}^{M} b_i u_s^{(0)}(t - iT_s) + \sum_{i=1}^{M+1} b_{i-1} u_s^{(1)}(t - iT_s) + w(t) \\ &= \sum_{i=0}^{M} \prod_{k=0}^{i} a_k q(t - iT_s) + \sum_{i=1}^{M+1} \prod_{k=0}^{i-1} a_k g(t - iT_s) + w(t), \end{aligned} \tag{7}$$

where both $q(t) \triangleq b_0 u_s^{(0)}(t)$ and $g(t) \triangleq b_0 u_s^{(1)}(t)$ have non-zero support T_s and contain the channel parameters, the timing offset and the initial channel symbol b_0.

Now, the fact that $q(t)$ and $g(t)$ are both unknown to the receiver suggests detecting the information symbols $\mathbf{a}$ following the GLRT rule. This amounts to maximizing the log-likelihood metric (LLM)

$$\begin{aligned} \Lambda\left[y(t)|\tilde{\mathbf{a}}, \tilde{q}(t), \tilde{g}(t)\right] &= 2\int_0^{(M+1)T_s} y(t)\tilde{s}(t)\mathrm{d}t \\ &\quad - \int_0^{(M+1)T_s} \tilde{s}^2(t)\mathrm{d}t \end{aligned} \tag{8}$$

over $\tilde{\mathbf{a}} = \left[\tilde{a}_1, \tilde{a}_2, \ldots, \tilde{a}_M\right]^{\mathrm{T}}$ and the finite-energy functions $\tilde{q}(t)$ and $\tilde{g}(t)$ with support in $[0, T_s]$, where

$$\tilde{s}(t) = \sum_{i=0}^{M} \prod_{k=0}^{i} \tilde{a}_k \tilde{q}(t - iT_s) + \sum_{i=1}^{M+1} \prod_{k=0}^{i-1} \tilde{a}_k \tilde{g}(t - iT_s) \tag{9}$$

is the signal corresponding to the trial values of $\tilde{\mathbf{a}}$, $\tilde{q}(t)$ and $\tilde{g}(t)$. Exploiting the finite support of $\tilde{q}(t)$ and $\tilde{g}(t)$ in $[0, T_s)$, we can obtain

$$\int_0^{(M+1)T_s} y(t)\tilde{q}(t - iT_s)\mathrm{d}t = \int_0^{T_s} y(t + iT_s)\tilde{q}(t)\mathrm{d}t, \tag{10}$$

$$\int_0^{(M+1)T_s} y(t)\tilde{g}(t - iT_s)\mathrm{d}t = \int_0^{T_s} y(t + iT_s)\tilde{g}(t)\mathrm{d}t, \tag{11}$$

and

$$\begin{aligned} &\int_0^{(M+1)T_s} \tilde{q}(t - iT_s)\tilde{g}(t - jT_s)\mathrm{d}t \\ &= \begin{cases} \int_0^{T_s} \tilde{q}(t)\tilde{g}(t)\mathrm{d}t, & i = j \\ 0, & i \ne j. \end{cases} \end{aligned} \tag{12}$$

Hence, using (10)–(11) yields

$$\int_0^{(M+1)T_s} y(t)\tilde{s}(t)\mathrm{d}t = \int_0^{T_s}\left[\tilde{q}(t)\sum_{i=0}^{M}\prod_{k=0}^{i}\tilde{a}_k y(t+iT_s)+\tilde{g}(t)\sum_{i=1}^{M+1}\prod_{k=0}^{i-1}\tilde{a}_k y(t+iT_s)\right]\mathrm{d}t, \quad (13)$$

whereas according to (12), we get

$$\begin{aligned}\int_0^{(M+1)T_s}\tilde{s}^2(t)\mathrm{d}t &= (M+1)\int_0^{T_s}\left[\tilde{q}^2(t)+\tilde{g}^2(t)\right]\mathrm{d}t \\ &\quad +2\sum_{i=0}^{M}\sum_{j=1}^{M+1}\prod_{k=0}^{i}\tilde{a}_k\prod_{l=0}^{j-1}\tilde{a}_l\int_0^{(M+1)T_s}\tilde{q}(t-iT_s)\tilde{g}(t-jT_s)\mathrm{d}t \\ &= (M+1)\int_0^{T_s}\left[\tilde{q}^2(t)+\tilde{g}^2(t)\right]\mathrm{d}t+2\sum_{i=1}^{M}\tilde{a}_i\int_0^{T_s}\tilde{q}(t)\tilde{g}(t)\mathrm{d}t. \quad (14)\end{aligned}$$

Therefore, substituting (13) and (14) into (8), the LLM takes the form (we drop the influent multiplicative factor $M+1$)

$$\begin{aligned}&\Lambda\left[y(t)|\tilde{\mathbf{a}},\tilde{q}(t),\tilde{g}(t)\right] \\ &= 2\int_0^{T_s}\left[\tilde{q}(t)z_1(t;\tilde{\mathbf{a}})+\tilde{g}(t)z_2(t;\tilde{\mathbf{a}})\right]\mathrm{d}t \\ &\quad -\int_0^{T_s}\left[\tilde{q}^2(t)+\tilde{g}^2(t)\right]\mathrm{d}t-2\eta(\tilde{\mathbf{a}})\int_0^{T_s}\tilde{q}(t)\tilde{g}(t)\mathrm{d}t, \quad (15)\end{aligned}$$

where

$$z_1(t;\tilde{\mathbf{a}}) \triangleq \frac{1}{M+1}\sum_{i=0}^{M}\prod_{k=0}^{i}\tilde{a}_k y(t+iT_s), \quad t\in[0,T_s), \quad (16)$$

$$z_2(t;\tilde{\mathbf{a}}) \triangleq \frac{1}{M+1}\sum_{i=1}^{M+1}\prod_{k=0}^{i-1}\tilde{a}_k y(t+iT_s), \quad t\in[0,T_s), \quad (17)$$

and

$$\eta(\tilde{\mathbf{a}}) \triangleq \frac{1}{M+1}\sum_{i=1}^{M}\tilde{a}_i. \quad (18)$$

Accordingly, the GLRT-based decision strategy on the information symbols $\mathbf{a}$ can be formulated as

$$\hat{\mathbf{a}} = \arg\max_{\tilde{\mathbf{a}}}\left\{\max_{\tilde{q}(t),\tilde{g}(t)}\left\{\Lambda\left[y(t)|\tilde{\mathbf{a}},\tilde{q}(t),\tilde{g}(t)\right]\right\}\right\}. \quad (19)$$

In order to solve (19), we first keep $\tilde{\mathbf{a}}$ fixed and compute the inner term

$$\Gamma\left[y(t)|\tilde{\mathbf{a}}\right] \triangleq \max_{\tilde{q}(t),\tilde{g}(t)}\left\{\Lambda\left[y(t)|\tilde{\mathbf{a}},\tilde{q}(t),\tilde{g}(t)\right]\right\}.$$

Toward this end, we can resort to standard variational techniques by letting $\tilde{q}(t) = q_0(t)+\lambda\varepsilon(t)$ and $\tilde{g}(t) = g_0(t)+\mu\rho(t)$, $q_0(t)$ and $g_0(t)$ being the optimum solutions to be found, and $\varepsilon(t)$ and $\rho(t)$ two generic functions with support in $[0,T_s)$. After taking the first-order derivatives of $\Lambda\left[y(t)|\tilde{\mathbf{a}},\tilde{q}(t),\tilde{g}(t)\right]$ with respect to λ and μ and setting them to zero, we get

$$\begin{cases}\left.\dfrac{\partial\Lambda\left[y(t)|\tilde{\mathbf{a}},\tilde{q}(t),\tilde{g}(t)\right]}{\partial\lambda}\right|_{\substack{\lambda=0\\ \mu=0}} \\ \quad = 2\displaystyle\int_0^{T_s}\left[z_1(t;\tilde{\mathbf{a}})-q_0(t)-\eta(\tilde{\mathbf{a}})g_0(t)\right]\varepsilon(t)\mathrm{d}t \\ \quad = 0, \quad \forall\varepsilon(t) \\ \left.\dfrac{\partial\Lambda\left[y(t)|\tilde{\mathbf{a}},\tilde{q}(t),\tilde{g}(t)\right]}{\partial\mu}\right|_{\substack{\lambda=0\\ \mu=0}} \\ \quad = 2\displaystyle\int_0^{T_s}\left[z_2(t;\tilde{\mathbf{a}})-g_0(t)-\eta(\tilde{\mathbf{a}})q_0(t)\right]\rho(t)\mathrm{d}t \\ \quad = 0, \quad \forall\rho(t).\end{cases} \quad (20)$$

This equation set is satisfied whenever

$$\begin{cases}q_0(t)+\eta(\tilde{\mathbf{a}})g_0(t) = z_1(t;\tilde{\mathbf{a}}) \\ \eta(\tilde{\mathbf{a}})q_0(t)+g_0(t) = z_2(t;\tilde{\mathbf{a}}),\end{cases} \quad (21)$$

that is,

$$q_0(t) = \frac{z_1(t;\tilde{\mathbf{a}})-\eta(\tilde{\mathbf{a}})z_2(t;\tilde{\mathbf{a}})}{1-\eta^2(\tilde{\mathbf{a}})}, \quad (22)$$

$$g_0(t) = \frac{z_2(t;\tilde{\mathbf{a}})-\eta(\tilde{\mathbf{a}})z_1(t;\tilde{\mathbf{a}})}{1-\eta^2(\tilde{\mathbf{a}})}. \quad (23)$$

Then, substituting the solutions (22)–(23) of (21) into (15) yields (up to an irrelevant multiplicative factor)

$$\Gamma\left[y(t)|\tilde{\mathbf{a}}\right] = \int_0^{T_s}\left[z_1^2(t;\tilde{\mathbf{a}})+z_2^2(t;\tilde{\mathbf{a}})-2\eta(\tilde{\mathbf{a}})z_1(t;\tilde{\mathbf{a}})z_2(t;\tilde{\mathbf{a}})\right]\mathrm{d}t. \quad (24)$$

Consequently, in line with (19) and with $\Gamma\left[y(t)|\tilde{\mathbf{a}}\right]$ given by (24), the proposed SLS-MSDD detection rule becomes

$$\hat{\mathbf{a}} = \arg\max_{\tilde{\mathbf{a}}}\left\{\Gamma\left[y(t)|\tilde{\mathbf{a}}\right]\right\}. \quad (25)$$

A few remarks about (24)–(25) are now in order.

(1) Let us take into account the optimal estimates of the unknown waveform segments $q(t)$ and $g(t)$ given by (22) and (23), respectively. Making use of

$$y(t+iT_s) = [q(t)+a_i g(t)]\prod_{k=0}^{i}a_k + w(t+iT_s), \quad t\in[0,T_s), \quad (26)$$

that can be easily derived from (7) and (16)–(17) turn out to be

$$\begin{aligned}z_1(t;\tilde{\mathbf{a}}) &= \frac{1}{M+1}\sum_{i=0}^{M}\prod_{k=0}^{i}\tilde{a}_k\prod_{l=0}^{i}a_l\left[q(t)+a_i g(t)\right] \\ &\quad +\frac{1}{M+1}\sum_{i=0}^{M}\prod_{k=0}^{i}\tilde{a}_k w(t+iT_s) \\ &= \varphi(\tilde{\mathbf{a}})q(t)+\xi(\tilde{\mathbf{a}})g(t) \\ &\quad +\frac{1}{M+1}\sum_{i=0}^{M}\prod_{k=0}^{i}\tilde{a}_k w(t+iT_s), \\ &\quad t\in[0,T_s), \quad (27)\end{aligned}$$

$$z_2(t;\tilde{\mathbf{a}}) = \frac{1}{M+1}\sum_{i=1}^{M+1}[g(t)+a_i q(t)]\prod_{k=0}^{i-1}\tilde{a}_k\prod_{l=0}^{i-1}a_l + \frac{1}{M+1}\sum_{i=1}^{M+1}\prod_{k=0}^{i-1}\tilde{a}_k w(t+iT_s) = \varphi(\tilde{\mathbf{a}})g(t)+\zeta(\tilde{\mathbf{a}})q(t) + \frac{1}{M+1}\sum_{i=1}^{M+1}\prod_{k=0}^{i-1}\tilde{a}_k w(t+iT_s), \quad t\in[0,T_s), \tag{28}$$

where

$$\varphi(\tilde{\mathbf{a}}) \triangleq \frac{1}{M+1}\sum_{i=0}^{M}\prod_{k=0}^{i}\tilde{a}_k\prod_{l=0}^{i}a_l,$$

$$\xi(\tilde{\mathbf{a}}) \triangleq \frac{1}{M+1}\sum_{i=0}^{M}a_i\prod_{k=0}^{i}\tilde{a}_k\prod_{l=0}^{i}a_l$$

and

$$\zeta(\tilde{\mathbf{a}}) \triangleq \frac{1}{M+1}\sum_{i=0}^{M}a_{i+1}\prod_{k=0}^{i}\tilde{a}_k\prod_{l=0}^{i}a_l.$$

Substituting (27)–(28) into (22)–(23) and assuming a high SNR, it can be found that

$$q_0(t) = \frac{[\varphi(\tilde{\mathbf{a}})-\eta(\tilde{\mathbf{a}})\zeta(\tilde{\mathbf{a}})]q(t)+[\xi(\tilde{\mathbf{a}})-\eta(\tilde{\mathbf{a}})\varphi(\tilde{\mathbf{a}})]g(t)}{1-\eta^2(\tilde{\mathbf{a}})}, \tag{29}$$

$$g_0(t) = \frac{[\varphi(\tilde{\mathbf{a}})-\eta(\tilde{\mathbf{a}})\xi(\tilde{\mathbf{a}})]g(t)+[\zeta(\tilde{\mathbf{a}})-\eta(\tilde{\mathbf{a}})\varphi(\tilde{\mathbf{a}})]q(t)}{1-\eta^2(\tilde{\mathbf{a}})}. \tag{30}$$

It can be observed from (29)–(30) that, for $\tilde{\mathbf{a}}\neq\mathbf{a}$, the optimal estimates $q_0(t)$ and $g_0(t)$ differ from the true $q(t)$ and $g(t)$ respectively. On the other side, whenever $\tilde{\mathbf{a}}=\mathbf{a}$ we get $\varphi(\mathbf{a})=1$ and $\xi(\mathbf{a})=\zeta(\mathbf{a})=\eta(\mathbf{a})$, and hence, the estimates $q_0(t)$ and $g_0(t)$ coincide with the desired segments $q(t)$ and $g(t)$, regardless of the values of $\eta(\mathbf{a})$.

(2) The occurrence of $\eta(\tilde{\mathbf{a}})$ in the objective function (24) adds considerably to the computational complexity of the detector. To simplify the implementation of the SLS-MSDD, a practical approach is to approximate $\eta(\tilde{\mathbf{a}})$ by zero[6] and remove it from (24), resulting in the simplified objective function

$$\bar{\Gamma}\left[y(t)|\tilde{\mathbf{a}}\right] = \int_0^{T_s}\left[z_1^2(t;\tilde{\mathbf{a}})+z_2^2(t;\tilde{\mathbf{a}})\right]\mathrm{d}t, \tag{31}$$

where $z_1(t;\tilde{\mathbf{a}})$ and $z_2(t;\tilde{\mathbf{a}})$ are given again by (16)–(17). Adopting (31) as the objective function in lieu of (24) means detecting the transmitted symbols by searching for the maximum of the sum of two partial energy metrics: the first is related to $z_1(t;\tilde{\mathbf{a}})$ and the other to $z_2(t;\tilde{\mathbf{a}})$. More specifically, whenever the SNR value is asymptotically large and so the assumption $\tilde{\mathbf{a}}=\mathbf{a}$ stands, evaluation of (27)–(28) leads to

$$\bar{\Gamma}\left[y(t)|\tilde{\mathbf{a}}\right]_{\tilde{\mathbf{a}}=\mathbf{a}} = \int_0^{T_s}\left[q^2(t)+g^2(t)\right]\mathrm{d}t = \int_0^{T_s}u_s^2(t)\mathrm{d}t, \tag{32}$$

that is, the maximum value of (31) in the asymptotic case is given by the energy of the received symbol-level waveform $u_s(t)$, independent of both the data symbol sequence $\mathbf{a}$ and the timing offset τ.

(3) The SLS-MSDD circumvents both the explicit estimation of the channel parameters and the need for accurate frame-level (or even pulse-level) timing synchronization. The metric (31) to be maximized, indeed, relies on the energy of $z_1(t;\tilde{\mathbf{a}})$ and $z_2(t;\tilde{\mathbf{a}})$, which can be constructed entirely from the received signal $y(t)$, as shown in (16)–(17).

(4) Since the information symbols take values in $\{\pm1\}$, the metric (31) can be further rearranged to an equivalent form that is suited for practical implementations of the SLS-MSDD. Similarly to the approach in [13], it is possible to show that

$$\bar{\Gamma}\left[y(t)|\tilde{\mathbf{a}}\right] = \sum_{i=1}^{M}\sum_{l=0}^{i-1}\prod_{k=1}^{i-l}\tilde{a}_{k+l}(Y_{l,i}+Y_{l+1,i+1}), \tag{33}$$

where the coefficients

$$Y_{i,j} \triangleq \frac{1}{M+1}\int_0^{T_s}y(t+iT_s)y(t+jT_s)\mathrm{d}t \tag{34}$$

are obtained by correlating symbol-long segments of the received signal $y(t)$ up to M symbols apart. It is worth noting that generation of $\{Y_{i,j}\}$ requires waveform storage with delays on the order of multiples of symbol intervals. This can be practically done via either analog averaging or digital sampling, even though both of them have drawbacks in terms of hardware implementation. Analog averaging requires long high-bandwidth delay lines that are hard to realize. Digital sampling requires accurate high-rate ADCs at Nyquist rates, which can be costly in terms of chip area and power consumption. Nevertheless, the latter approach can be affordable using low-resolution samplers as suggested by the study in [24] on UWB receiver implementation. As an alternative, one might also consider subsampling techniques for direct signal conversion [25] or use subsampling combined with sparsity considerations to reconstruct the high bandwidth signal [26,27], thus trading off performance against complexity.

(5) The basic idea of the SLS-MSDD is to jointly detect a block of M data symbols, within which the channel response can be considered as time-invariant. As a result, the detection accuracy is expected to improve as M increases. Finding out the maximum of the objective function (33) via some exhaustive search method, however, requires high computational complexity going up exponentially in the number of symbols M to be jointly detected. Therefore, whenever performance

[6] This approximation is accurate when information-bearing symbols are independent and identically distributed, in which case their mean value $\eta(\tilde{\mathbf{a}})$ approaches 0 as the data size M increases. Nevertheless, there exists a (limited) percentage of symbol sequences for which $|\eta(\tilde{\mathbf{a}})| \ll 1$ is not fulfilled. To make this condition more rigorous, some form of information symbol precoding could help, although it is out of the scope of the current paper.

has to be attained at affordable complexity, efficient implementations of the SLS-MSDD are inevitably called for, which will be the focus of next section.

4. Sphere decoding for SLS-MSDD

An effective way to elude the expensive computational load required by the exhaustive-search-based SLS-MSDD is to take advantage of the SD algorithm. Originally proposed to solve the so-called shortest vector problem (SVP) in a lattice [23], the SD basically relies upon examining only those lattice points (assumed to belong to a given finite-alphabet) inside a sphere of radius δ, which is progressively made smaller and smaller to reduce the search space, thereby lessening the overall computational complexity. The SLS-MSDD detection rule developed so far, however, does not yet fit in the SD framework, and accordingly, a proper reformulation of the objective function $\bar{\Gamma}\left[y(t)|\tilde{\mathbf{a}}\right]$ in (33) is required. To this end, a key observation we make here is that the maximum possible value of (33) is independent of $\tilde{\mathbf{a}}$ as long as they take values in $\{\pm 1\}$, that is,

$$\bar{\Gamma}_{\mathrm{MAX}}\left[y(t)\right] \triangleq \sum_{i=1}^{M}\sum_{l=0}^{i-1}\left|Y_{l,i}+Y_{l+1,i+1}\right|. \tag{35}$$

Hence, subtracting (33) from (35), the new objective function (this time to be minimized) becomes

$$\Phi\left[y(t)|\tilde{\mathbf{a}}\right] = \sum_{i=1}^{M}\sum_{l=0}^{i-1}\vartheta_{l,i}\left|Y_{l,i}+Y_{l+1,i+1}\right|, \tag{36}$$

where

$$\vartheta_{l,i} \triangleq 1-\sigma_{l,i}\prod_{k=1}^{i-l}\tilde{a}_{k+l} \tag{37}$$

takes values in $\{0, 2\}$ depending on whether $\sigma_{l,i} \triangleq \mathrm{sign}\{Y_{l,i}+Y_{l+1,i+1}\}$ has the same or opposite sign with respect to $\prod_{k=1}^{i-l}\tilde{a}_{k+l}$. According to (36)-(37), the SLS-MSDD can thus be put in the alternative form

$$\hat{\mathbf{a}} = \arg\min_{\tilde{\mathbf{a}}}\left\{\Phi\left[y(t)|\tilde{\mathbf{a}}\right]\right\}, \tag{38}$$

which is structurally amenable to be put into practice through the SD search algorithm for the following reasons: (i) the objective function (36) is nothing but the sum of the non-negative coefficient $\left|Z_{l,i}\right|$, with $Z_{l,i} \triangleq Y_{l,i}+Y_{l+1,i+1}$, weighted linearly by the non-negative integer-valued unknowns $\vartheta_{l,i}$; (ii) the i-th addend in (36), $\sum_{l=0}^{i-1}\vartheta_{l,i}\left|Z_{l,i}\right|$, depends on the preceding tentative symbols up to $\tilde{a}_i$, namely, $\tilde{a}_1, \tilde{a}_2, \ldots, \tilde{a}_i$; (iii) in view of (i)–(ii), (36) defines a sphere in the M-dimensional lattice of the trial vectors $\tilde{\mathbf{a}} \triangleq [\tilde{a}_1, \tilde{a}_2, \ldots, \tilde{a}_M]^{\mathrm{T}}$ [28], which fully complies with the SD framework.

Based on the above observations, we now illustrate how to realize the SD-based SLS-MSDD. For the sake of simplicity, assume that the initial radius $\delta^{(1)} > 0$ is chosen to be large enough so that the sphere defined by (36) contains the optimal $\hat{\mathbf{a}}$ to be searched for. As the generic m-th SD iteration, a *necessary condition* for any tentative estimate $\hat{\mathbf{a}}^{(m)}$ to lie inside the sphere of radius $\delta^{(m)} > 0$ is given by

$$\sum_{i=1}^{j}\sum_{l=0}^{i-1}\left[1-\sigma_{l,i}\prod_{k=1}^{i-l}\hat{a}_{k+l}^{(m)}\right]\left|Z_{l,i}\right| \le \delta^{(m)}, \quad 1 \le j \le M, \tag{39}$$

or more explicitly,

$$j=1: \left[1-\sigma_{0,1}\hat{a}_1^{(m)}\right]\left|Z_{0,1}\right| \le \delta^{(m)}; \tag{40a}$$

$$j=2: \left[1-\sigma_{0,1}\hat{a}_1^{(m)}\right]\left|Z_{0,1}\right| + \left[1-\sigma_{0,2}\hat{a}_1^{(m)}\hat{a}_2^{(m)}\right]\left|Z_{0,2}\right| + \left[1-\sigma_{1,2}\hat{a}_2^{(m)}\right]\left|Z_{1,2}\right| \le \delta^{(m)}; \tag{40b}$$

$$\vdots$$

$$j=M: \sum_{i=1}^{M}\sum_{l=0}^{i-1}\left[1-\sigma_{l,i}\prod_{k=1}^{i-l}\hat{a}_{k+l}^{(m)}\right]\left|Z_{l,i}\right| \le \delta^{(m)}. \tag{40c}$$

Interesting to note, the condition (40a) for $j = 1$ contains $\hat{a}_1^{(m)}$ only, (40b) concerning $j = 2$ contain $\hat{a}_1^{(m)}$ and $\hat{a}_2^{(m)}$ only, and so on. This suggests checking the M conditions in (39) one by one at each iteration of the SD algorithm, as summarized in the following steps.

S_1: starting with (40a), the candidate set for $\hat{a}_1^{(m)}$ can be found as

$$\mathcal{I}_1^{(m)} = \left\{\tilde{a}_1 \in \{\pm 1\} | (1-\sigma_{0,1}\tilde{a}_1)\left|Z_{0,1}\right| \le \delta^{(m)}\right\}; \tag{41}$$

S_2: after the tentative $\hat{a}_1^{(m)}$ has been chosen from $\mathcal{I}_1^{(m)}$, it is substituted into (40b) to produce the candidate set for $\hat{a}_2^{(m)}$ as

$$\mathcal{I}_2^{(m)} = \left\{\tilde{a}_2 \in \{\pm 1\} \left| \left[1-\sigma_{0,1}\hat{a}_1^{(m)}\right]\left|Z_{0,1}\right| + \left[1-\sigma_{0,2}\hat{a}_1^{(m)}\tilde{a}_2\right]\left|Z_{0,2}\right| + \left[1-\sigma_{1,2}\tilde{a}_2\right]\left|Z_{1,2}\right| \le \delta^{(m)}\right.\right\}; \tag{42}$$

$$\vdots$$

S_j: the candidate set $\mathcal{I}_j^{(m)}$ for $\hat{a}_j^{(m)}$ is based on the tentative decisions $\{\hat{a}_1^{(m)}, \hat{a}_2^{(m)}, \ldots, \hat{a}_{j-1}^{(m)}\}$ and equals

$$\mathcal{I}_j^{(m)} = \left\{\tilde{a}_j \in \{\pm 1\} | \left[1-\sigma_{0,1}\hat{a}_1^{(m)}\right]\left|Z_{0,1}\right| + \left[1-\sigma_{0,2}\hat{a}_1^{(m)}\hat{a}_2^{(m)}\right]\left|Z_{0,2}\right| + \left[1-\sigma_{1,2}\hat{a}_2^{(m)}\right]\left|Z_{1,2}\right| + \cdots + \left[1-\sigma_{0,j}\hat{a}_1^{(m)}\hat{a}_2^{(m)}\cdots\tilde{a}_j\right]\left|Z_{0,j}\right| + \left[1-\sigma_{1,j}\hat{a}_2^{(m)}\hat{a}_3^{(m)}\cdots\tilde{a}_j\right]\left|Z_{1,j}\right| + \left[1-\sigma_{j-1,j}\tilde{a}_j\right]\left|Z_{j-1,j}\right| \le \delta^{(m)}\right\}; \tag{43}$$

$$\vdots$$

S_M: the last candidate set $\mathcal{A}_M^{(m)}$ is acquired for $\hat{a}_M^{(m)}$, which concludes the m-th iteration. Then, the radius $\delta^{(m)}$ and the optimal estimate $\hat{\mathbf{a}}_{\text{opt}}$ are updated according to the new tentative estimate $\hat{\mathbf{a}}^{(m)}$

$$\delta^{(m+1)} \leftarrow \Phi\left[y(t)|\hat{\mathbf{a}}^{(m)}\right], \tag{44a}$$

$$\hat{\mathbf{a}}_{\text{opt}} \leftarrow \hat{\mathbf{a}}^{(m)}, \tag{44b}$$

and further, the next $(m+1)$-th iteration follows.

The iterations go on with a smaller and smaller sphere, with the candidate estimate $\hat{\mathbf{a}}^{(m)}$ found in the previous iteration lying on its surface. When at a given iteration all nodes have been visited without any success, the iterative process stops, yielding the optimal solution $\hat{\mathbf{a}}_{\text{opt}}$ for which the objective function attains the minimum value $\Phi\left[y(t)|\hat{\mathbf{a}}_{\text{opt}}\right]$.

Several remarks are now of interest.

(1) The proposed SD-based SLS-MSDD shares with the SD of the existing literature optimal ML performance at *polynomial* complexity (often cubic or higher) in the data block size over a wide range of practical SNRs, as will be verified in Section 5.4.
(2) At a given iteration index m and for some symbol index j, the candidate set $\mathcal{A}_j^{(m)}$ for $\hat{a}_j^{(m)}$ might be empty. In that case, a new iteration starts immediately by decrementing the index j and testing a different value for $\hat{a}_j^{(m+1)}$.
(3) The choice of the initial radius $\delta^{(1)}$ is critical, and can add to the overall complexity if not properly addressed. Indeed, if it is chosen too small, no point lies inside the sphere and the algorithm must restart with a larger radius, whereas, if chosen too large, many more points have to be checked. A reasonable choice is to set the initial radius by evaluating (36) in correspondence with a given tentative sequence, for instance that with pseudo-random binary distributed entries.
(4) To speed up the search procedure, at each iteration $\hat{a}_j^{(m)}$ is picked up from $\mathcal{A}_j^{(m)}$ so that the metric to be evaluated in (39) is minimized. So doing, the SD search space is reduced, and accordingly, computational complexity gets remarkably lower.
(5) Since the unknown $\vartheta_{l,i}$ takes integer values in $\{0, 2\}$, checking the M conditions in (39) requires no multiplications, but simply real additions combined with logical operations.
(6) The real-valued coefficients $|Z_{l,i}|$ depend on the received signal through (34), and therefore, can be pre-computed before the SD iterations start. As an alternative, we can employ only the sign of $Z_{l,i}$ by substituting $|Z_{l,i}| = 1$ in (40a)–(40c). This strategy leads to the one-bit hard-quantized version of the SLS-MSDD, which allows a further reduction in complexity in that simpler integer-format additions and logical operations are now required.

5. Performance results

In this section, the effectiveness of the SD-based SLS-MSDD receiver is verified over dense multipath wireless environments through computer simulations. First, the BER performance is quantified as a function of the ratio $E_b/\mathcal{N}_0$ in both single-user and MAI scenarios, E_b being defined as the mean received energy per transmitted bit. Next, some implementation issues are investigated with particular emphasis on the savings in computational complexity which can be obtained with respect to the SLS-MSDD based on exhaustive search (ES). The following conventional schemes are taken as performance benchmarks: (i) single-user Rake receiver with perfect channel state information (CSI) and ideal timing recovery (IRake); (ii) single-user symbol-by-symbol DD with ideal timing recovery (IDD); (iii) single-user symbol-by-symbol DD with symbol-level synchronization (SLS-DD).

5.1. Simulation setup

In the system setup for all simulation runs, each active user transmits consecutive bursts of M binary PAM information-bearing symbols. The transmission channel is assumed to be time-invariant within each burst, but randomly varying from burst to burst according to the model in [29]. To be specific, the multipath components arrive in clusters with amplitudes modeled as independent double-sided Rayleigh distributed random variables having mean square values exponentially decaying with the cluster delays, as well as with the ray delays within the cluster, with decay factors chosen as 30 ns and 5 ns, respectively. The clusters and the rays within each cluster have Poisson distributed arrival times with arrival rates 0.5 ns^{-1} and 2 ns^{-1}, respectively. The monocycle $p(t)$ is selected as the second derivative of a Gaussian shape with normalized unit energy and pulse width equal to $T_p = 1.0$ ns. The frame and chip interval are $T_f = 100$ ns and $T_c = 1.0$ ns, respectively, $N_f = 10$ is the number of frames per information symbol, while the TH codes c_j are randomly picked in the interval $[0, N_c - 1]$ with $N_c = 91$, so that $c_j T_c < T_f, \forall j \in [0, N_f - 1]$. In the MAI scenario, the $N_u - 1$ interfering users have the same power P_i, whereas the desired one has power P_u, so that the near/far ratio (NFR) results as NFR $\triangleq P_i/P_u$. Further, the time origins of all the active users are set randomly over the symbol interval $(0, T_s)$ to reproduce an asynchronous access to the channel and in line with the assumption that the timing information of the desired user is acquired at the symbol level only.

5.2. BER in the single-user scenario

Fig. 1 illustrates the BER performance of the SLS-MSDD in a single-user scenario ($N_u = 1$) with the coefficients $Z_{l,i}$ taken as real-valued values (soft SD), and for different block sizes, namely, $M = 5, 10, 15, 20, 30, 35$. As expected, the performance of the SLS-MSDD improves as the block size M increases: at BER $= 10^{-2}$, the performance gap between the $M = 5$ scheme and that with $M = 10$ is more than 6 dB, while $M = 35$ offers an additional gain of 5 dB over $M = 10$. When M is not large enough, however, the BER curves exhibit noise floors in the high SNR region, due to insufficient averaging that compromises the assumption $\eta(\mathbf{a}) \approx 0$ we made to reduce the detector complexity.

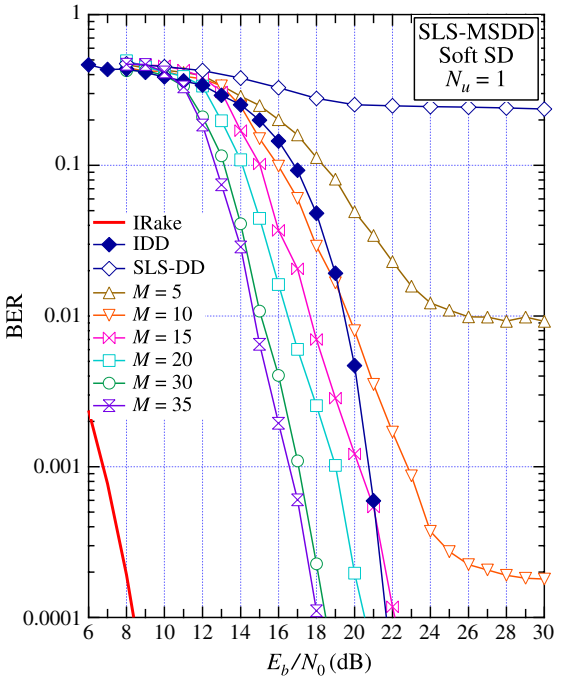

Fig. 1. BER of SLS-MSDD with soft SD metrics for $N_u = 1$ and various M.

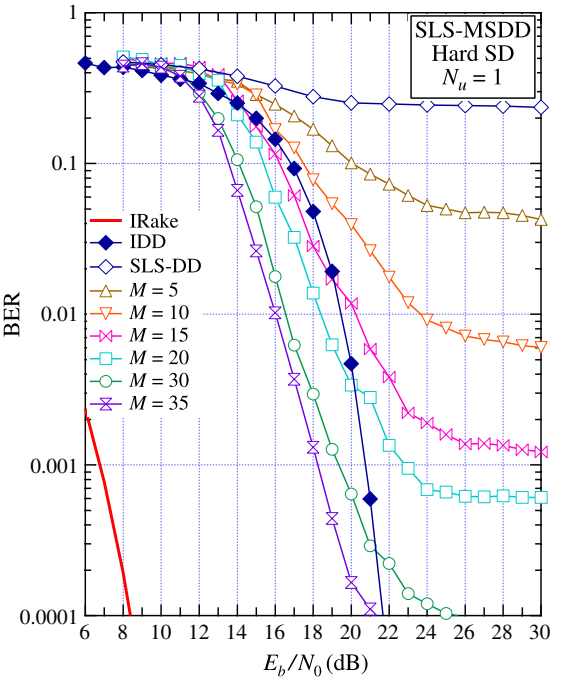

Fig. 2. BER of SLS-MSDD with hard SD metrics for $N_u = 1$ and various M.

The above phenomenon is considerably alleviated as M increases. Still, the SLS-MSDD has a significant edge compared to the conventional DD scheme not only with mistiming (SLS-DD) but also with ideal timing recovery (IDD). In fact, the gain of the SLS-MSDD with $M = 35$ over the IDD is more than 5 dB in the BER interval of practical interest while skipping accurate timing synchronization. On the other side, the IRake outperforms the SLS-MSDD by approximately 10 dB, but at a very expensive price paid for accurate channel and timing estimation.

Fig. 2 refers to the SLS-MSDD in the single-user case with one-bit hard-quantized coefficients $Z_{l,i}$ (hard SD). In accordance with Fig. 1, the BER metrics improve with the data block size M, flatten out in the high-SNR region at moderate M, and are still superior to those of both the SLS-DD and IDD. Nevertheless, the considerable reduction in computational complexity due to the adoption of integer-based arithmetic only has to be inevitably traded with a given performance degradation. If compared to the soft version, this is limited, however, to 1–2 dB only, providing that the burst length takes adequate values, say $M \geq 15$.

5.3. BER in the MAI scenario

The BER curves of Fig. 3 quantify the MAI effects on the soft version of the SLS-MSDD when the block size is $M = 20$ (square marks) or $M = 30$ (circle marks), the number of active users is $N_u = 5$, 10, 15 and the NFR parameter is set to -6 dB. The single-user cases for both the SLS-MSDD and the conventional IDD are also plotted as reference. As one could expect, the BER performance gets worse as the MAI level increases. At BER $= 10^{-2}$, the SLS-MSDD with $M = 30$ can sustain $N_u = 5$ users at a small price of less than 0.5 dB in extra SNR (compared to the single-user case),

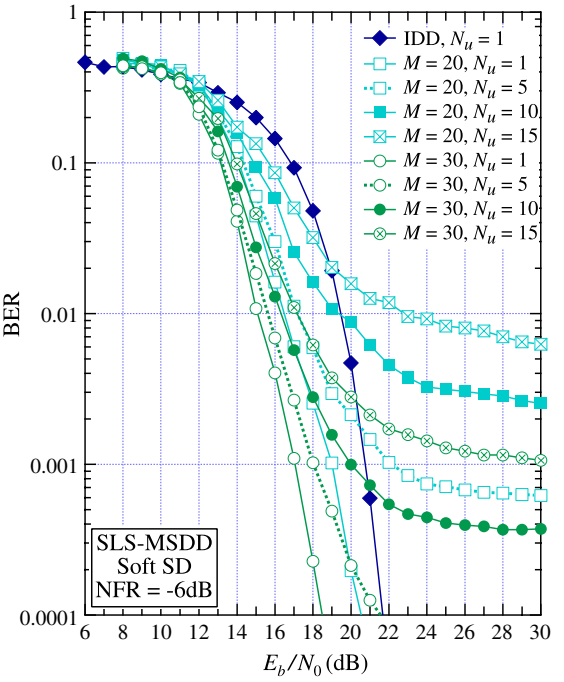

Fig. 3. BER of SLS-MSDD with soft SD metrics for $M = 20$, 30, NFR $= -6$ dB, and various N_u.

whereas 2 dB has to be expended additionally when the MAI level raises to $N_u = 15$. Further, the BER robustness of the SLS-MSDD against the MAI improves adopting a longer data block. At BER $= 10^{-2}$, the SLS-MSDD using $M = 20$ outperforms the IDD operating in a single-user channel up

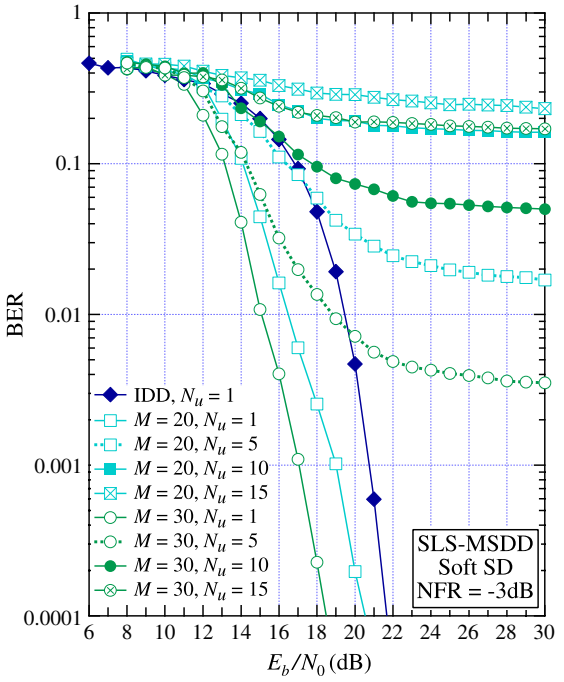

Fig. 4. BER of SLS-MSDD with soft SD metrics for $M = 20, 30$, NFR $= -3$ dB, and various N_u.

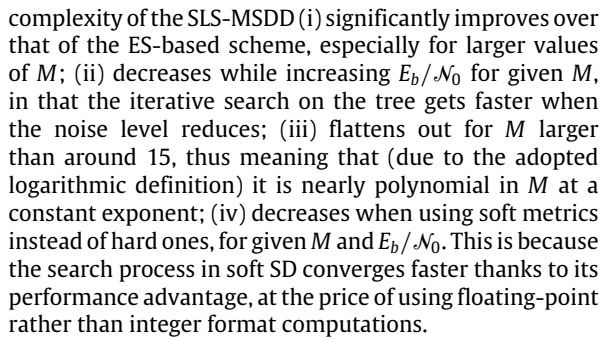

Fig. 5. Complexity exponent of SLS-MSDD with soft and hard SD metrics for $N_u = 1$.

to $N_u = 10$ users, whereas the same can be achieved at a lower BER of 10^{-3} as well, as long as $M = 30$ is employed.

When the NFR in multi-user scenario increases to -3 dB, the MAI effects turn out to be much stronger, as shown in Fig. 4. When $N_u = 5$, the SLS-MSDD can reach the BER level of 10^{-2} only provided that the block size is set to $M = 30$, while choosing $M = 20$ the BER increases to (asymptotically) around 2×10^{-2}. Setting the number of active users to $N_u = 15$, instead, significantly degrades the SLS-MSDD performance in that the BER plots for both $M = 20$ and $M = 30$ flatten out above the 0.1 level.

5.4. Computational complexity

The computational load of the SD-based SLS-MSDD can be derived from the total number of additions spent in evaluating the conditions (39) throughout the iterations required by the search procedure. Depending on not only the data block size M (or equivalently, how many nodes are included in the tree to be visited) but also the received signal (which affects the sphere radius chosen at each iteration), the complexity is a random variable that has to be properly described through its average properties. In the sequel, adhering to the approach followed in [28], we will refer to the so-called complexity exponent (CE), defined as the logarithm of base M of the average number of flop operations per data block.

The CE metric is illustrated in Fig. 5 as a function of M and for various $E_b/\mathcal{N}_0$ ratios, for both the soft (solid lines) and hard (dotted lines) versions of the SLS-MSDD operating in the single-user scenario. We also included the CE of the SLS-MSDD based on ES (solid line without marks) as a performance benchmark. The results suggest that the complexity of the SLS-MSDD (i) significantly improves over that of the ES-based scheme, especially for larger values of M; (ii) decreases while increasing $E_b/\mathcal{N}_0$ for given M, in that the iterative search on the tree gets faster when the noise level reduces; (iii) flattens out for M larger than around 15, thus meaning that (due to the adopted logarithmic definition) it is nearly polynomial in M at a constant exponent; (iv) decreases when using soft metrics instead of hard ones, for given M and $E_b/\mathcal{N}_0$. This is because the search process in soft SD converges faster thanks to its performance advantage, at the price of using floating-point rather than integer format computations.

6. Concluding remarks

The aim of the current paper has been to derive a novel multi-symbol detector for UWB communications with remarkable robustness to mistiming. A number of appealing features are offered: (i) joint data detection based on symbol-level synchronization only, (ii) simple receiver structure by circumventing the costly tap-by-tap channel estimation required by conventional coherent schemes, and (iii) efficient implementation by resorting to a sphere decoding approach which enables affordable computational complexity even for large blocks. Simulation results obtained for typical dense multipath channels in both single-user and MAI-limited scenarios indicate that the adoption of a proper block size enables attractive performance-versus-complexity tradeoffs.

References

[1] R.A. Scholtz, M.Z. Win, Impulse radio: How it works, IEEE Commun. Lett. 2 (2) (1998) 36–38.
[2] L. Yang, G.B. Giannakis, Ultra-wideband communications: An idea whose time has come, IEEE Signal Process. Mag. 21 (6) (2004) 26–54.